Journal of Cluster Science (2020) 31:887–896
https://doi.org/10.1007/s10876-020-01760-4

ORIGINAL PAPER

Synthesis, Structure and Photoluminescence Analysis of a Ho^{3+}-cluster-based 3D coordination polymer: $\{Ho_2(H_2O)_2(DMF)_2(ATPA)_3\}_n$

Adem Dönmez[1,2]

Received: 25 October 2019 / Published online: 14 January 2020

Abstract

A new Ho(III) cluster-based 3D coordination polymer with the formula $\{Ho_2(H_2O)_2(DMF)_2(ATPA)_3\}_n$ (H_2ATPA = 2-Aminoterephthalic acid, DMF = *N*,*N*-dimethylformamide), **1**, has been successfully synthesized via the hydrothermal method and characterized by elemental analysis, FT-IR, UV, single crystal and powder X-ray diffraction and photoluminescence measurements. Each Holmium atom has a distorted bicapped trigonal prismatic geometry with coordination of eight oxygen atoms. The shifting of the absorption band in the UV–Visible spectrum of **1** indicates the Ho atoms involved in coordination with H_2ATPA ligand. Ho(III)-based characteristic narrow strong emission bands due to the f–f transitions of Ho(III) cation have been detected for **1** in the visible region. The emission bands observed at 442 nm and 464 nm are the most severe, so the investigated complex emits the bright-blue light. One can conclude that the energy transfers from the H_2ATPA ligand to Ho(III) have been done effectively so that **1** would have the potential applications in the optical amplification field.

Keywords Ho(III) · X-ray structure · Luminescence · 2-Aminoterephthalic acid

Introduction

The discovery of novel functional materials has a very important role in the development of science and technology. In recent years, metal–organic frameworks (MOFs) also known as porous coordination polymers (CPs) are one of the most prominent groups of functional materials due to their tunable structural and electronic properties by changing the organic/inorganic metal ions/clusters with organic linkers and the metal nodes [1–4]. Furthermore, unique features of MOFs, such as extremely large surface area, uniform and tunable pore size enable a widened use of them for many applications, including catalysis [5], chemical sensing [6], gas storage/separation [7], drug delivery [8], and contrast agent [9].

One special type of MOFs based on trivalent lanthanides (LnMOFs) as multifunctional systems have attracted wide interest for their high thermal and chemical stability and luminescent output [10–14]. LnMOFs have advantages in that they have the following aspects: (i) the variety of lanthanide ions as the nodes and numerous organic linkers to form LnMOFs have made a great promise to produce a large amount of new luminescent material, (ii) it is possible to incorporate of different lanthanide ion into the same host due to the isostructural chemistry of LnMOFs to successfully achieve tunable luminescence properties, (iii) "luminescence sensitization" also known as "antenna effect" can be widely explored by coordination of Ln^{3+} ions with suitable conjugated chromophores that participate in energy transition processes, and (iv) the coupling between photoluminescence and magnetism sets the scene for scientists interested in LnMOFs [15, 16].

The advantages of LnMOFs due to intrinsic luminescent features of lanthanides offer excellent prospects to design novel functional luminescent materials. Lanthanide elements have a rich variety of electronic energy levels

Electronic supplementary material The online version of this article (https://doi.org/10.1007/s10876-020-01760-4) contains supplementary material, which is available to authorized users.

✉ Adem Dönmez
adonmez@mu.edu.tr

[1] Department of Physics, Faculty of Science, Molecular Nano-Materials Laboratory, Mugla Sıtkı Koçman University, 48170 Mugla, Turkey

[2] Scientific Research Projects Coordination Unit, Mugla Sitki Kocman University, Mugla, Turkey

because of the unfilled 4f shells, resulting in the intrinsic luminescent features [15]: (i) strong long excited-state luminescence lifetimes (up to several hundreds of microsecond due to shielding of 4f electrons of lanthanide ions from the external interactions by the outer shells of $5s^2$ and $5p^6$, resulting high purity color of materials and devices, (ii) high luminescence quantum yield in the near-infrared, providing high sensitivity in sensor applications [17], (iii) large ligand-induced Stokes shifts to avoid self-quenching [18], and (iv) characteristic sharp emission peaks observed from the fluorescence profiles.

Up to now, a large number of LnMOFs with different geometries and topologies have been designed to be used in various potential applications. For example, Ma et al. [19] reported that a series of isostructural LnMOFs, PCN-17 (Dy, Er, Y, Yb) based on novel square-planar $Ln_4(\mu_4\text{-}H_2O)$ SBUs, exhibit selective gas adsorption of H_2 and O_2 over N_2 and CO, promises its potential in gas separation applications. Abdelhamid et al. [20] reported that another series LnMOFs, denoted as SUMOF-7II (Ln) and SUMOF-7IIB (Ln) (Ln = La, Ce, Pr, Nd, Sm, Eu, and Gd) with different linkers, promise their applications in biosensing and telecommunications. As another example, Du et al. [21] investigated a 3D LnMOF with the formula $[Nd_2(abtc)_{1.5}(H_2O)_3(DMA)]\cdot H_2O\cdot DMA$ (DMA = *N*,*N*-dimethylacetamide) to make a promising drug delivery host material.

As seen from the examples above, most studies focused on LnMOFs include La(III), Nd(III), Sm(III), Eu(III), Gd(III) and Dy(III) compounds. But detailed analyses on Ho(III) complexes are still rare. Ho(III) activated luminescent materials are a great interest of potential applications as single-phase white phosphors emitting light with high color purity within all range of the visible spectrum. The properties of Ho(III) activated phosphors with multicolor emission may be improved by the coordination of ligands to enhance the efficiency of emission. Ambidentate 2-aminoterephthalic acid (H_2ATPA) is a good candidate for this purpose. H_2ATPA was chosen as a ligand in this study by considering the presence of hydrogen-bonding donor and acceptor sites provided by amino groups in H_2ATPA, to make CP functional [22]. Also, H_2ATPA has two carboxyl groups, establishing bridges between several metal nodes as a rigid linker to stabilize the structure with open frameworks [23].

Considering that much basic knowledge is still needed in the research area of LnMOFs, this study was motivated to build and characterized a new Ho^{3+} cluster-based 3D coordination polymer with the formula $\{Ho_2(H_2O)_2(DMF)_2(ATPA)_3\}_n$ (H_2ATPA = 2-aminoterephtlatic acid, DMF = *N*,*N*-dimethylformamide). One of the most common methods of the hydrothermal technique was used to synthesize the sample for a good crystallinity. The structural and luminescence properties of the sample were examined in detail to provide a better understanding of the photoluminescence processes in LnMOFs. A variety of experimental techniques like X-ray diffraction, room temperature solid-state UV, FT-IR, and photoluminescence spectroscopy used to reveal the structural and luminescence properties, respectively.

Experimental Equipment and Conditions

All the chemicals were used as received without any further purification. Elemental (C, H, N) analyses were carried out using a LECO, CHNS–932. FT-IR spectra were collected in the region from 600 to 4000 cm^{-1} using a Perkin Elmer Spectrum 65 FT-IR spectrometer. The solid-state UV–Vis spectra were observed by an Ocean Optics Maya 2000Pro UV–vis Spectrometer. The photoluminescence measurements were performed at room temperature by using ANDOR SR500i-BL Photoluminescence Spectrometer with Nd:YLF laser. A constant laser wavelength of 349 nm was kept and 1.3 mJ and 5 ns pulse width energy per pulse was applied to the laser source during the experiments.

Single crystal X-ray diffraction patterns were collected at 293 K using an Xcalibur, Eos diffractometers with graphite monochromatic Mo–Kα radiation (λ = 0.71073 Å). The crystal structure was solved by a standard direct method using the SHELX program [24]. A method of full-matrix least-squares on F^2 using the SHELXL program [25] using the OLEX2 software [26] was adopted for the refinement. The hydrogen atoms were positioned ideally and refined with individual isotropic displacement parameters using the riding model whereas all non-hydrogen atoms were refined anisotropically. A summary of the crystal data and refinement results is given in Table 1. A schematic representation of **1** is shown in Scheme 1.

Synthesis

The synthesis route consists of four processes as indicated in Scheme 2. In the first process for the synthesis of the polymeric sample; $Ho(NO_3)_3.5H_2O$, (0.0441 g, 0.1 mmol) and 2-Aminoterephthalic acid (0.0181 g, 0.1 mmol) were directly dissolved in 10 mL of distilled water and 10 mL of dimethylformamide (DMF), respectively. Then, two obtained solutions were mixed by simultaneous pouring into a third glass vessel under vigorous stirring for 2 h. The pH of mixture solution was adjusted about 5 by adding NaOH solution (1 $mol\cdot L^{-1}$) drop by drop. The final mixture was sealed into a bomb equipped with a Teflon liner (45 mL) and then placed in the temperature and micro-time controller convection oven for 52 h at 140 °C. After cooling to room temperature naturally, the reactant mixture

Table 1 Crystal data and structure refinement information for **1**

Chemical formula	$C_{30}H_{30}Ho_2N_5O_{16}$
Formula weight (g mol^{-1})	1046.45
Crystal system	Triclinic
Space group	$P-1$
Unit cell dimensions	a = 8.1729 (4) Å; α = 114.530 (5)°
	b = 10.2482 (6) Å; β = 99.088 (4)°
	c = 11.6781 (6) Å; γ = 99.297 (4)°
V/Å^3	850.13 (9)
Z	1
ρ_{calc}/g cm^{-3}	2.04
μ/mm^{-1}	4.70
Crystal size (mm)	0.52 × 0.44 × 0.21
Temperature (K)	293
Reflections collected	5754
Independent reflections	3467
Goodness–of–fit on F^2	1.05
R indices [$I > 2\sigma(I)$]	R_1 = 0.030, wR_2 = 0.063

was washed several times with distilled water in order to remove the excess of residue. Anal. Calcd for $C_{30}H_{30}Ho_2N_5O_{16}$ (**1**): Calcd. C, 34.43; H, 2.89; N, 6.69%; Found: C, 34.40; H, 2.88; N, 6.68%; Yield: 63%.

Result and Discussion

Crystal Structure Description

The title complex crystallizes in a triclinic space group P-1 with unit cell parameters summarized in Table 1. The asymmetric unit of **1** is consist of one Holmium atom, coordinated one and a half aminoterephthalic acid (H_2-ATPA), one water, and one DMF molecule (Fig. 1). The Ho ion is eight coordinated by O1–O4, O7 and O8 atoms belong to three carboxylic groups of H_2ATPA ligands, O6 atom of water molecule and O5 atom of DMF molecule and have a distorted bicapped trigonal prismatic geometry (Fig. 2). The Ho–O bond distances are in the range of 2.323(3)–2.467(3) Å and the O–Ho–O angles are in the range of 53.76 (11)–153.30 (13)° (Table 2). All bond distance and angles resemble in those reported earlier structures [11–14]. In the structure of **1**, the 2-aminoterephthalic acid (H_2ATPA) exhibits two different tetradentate coordination modes (Fig. 2): the mode (a) μ-(η_2:η_2), where two oxygen atoms of one carboxylic group chelate one Ho(III) ion; the mode (b) μ_4-($\eta1$:$\eta1$:$\eta1$:$\eta1$), where the aminoterephthalate dianion coordinates four Ho(III) ions by each available oxygen atoms proceeding from two carboxylate groups [27]. In addition, the H_2ATPA linker

Scheme 1 Schematic representation of **1**

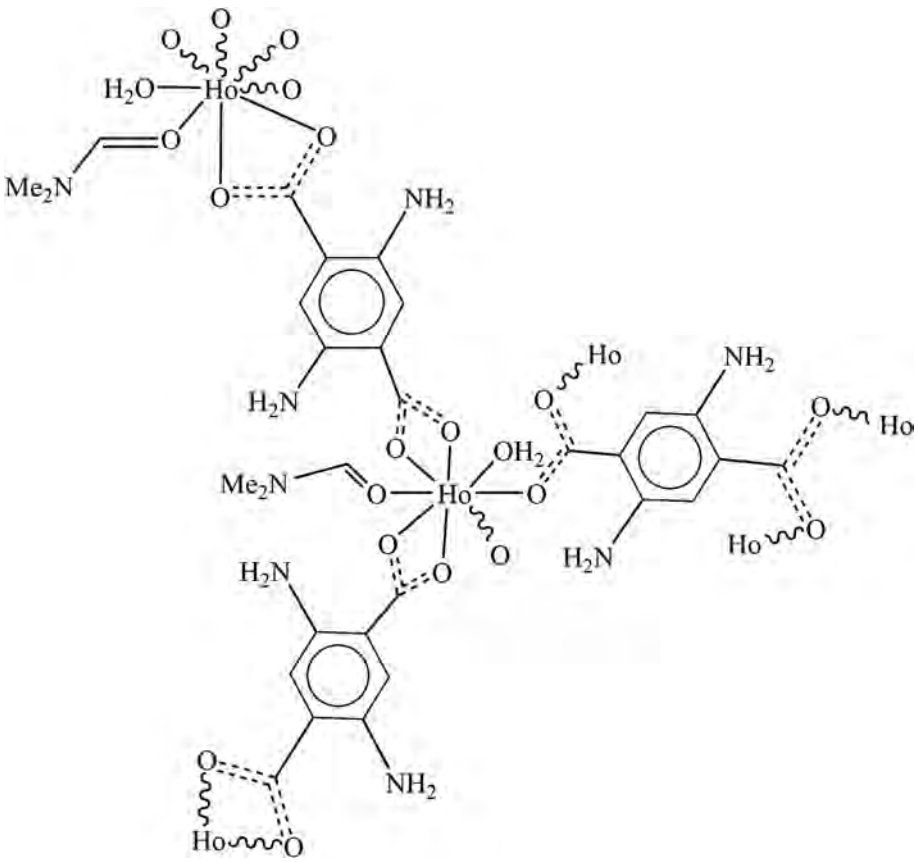

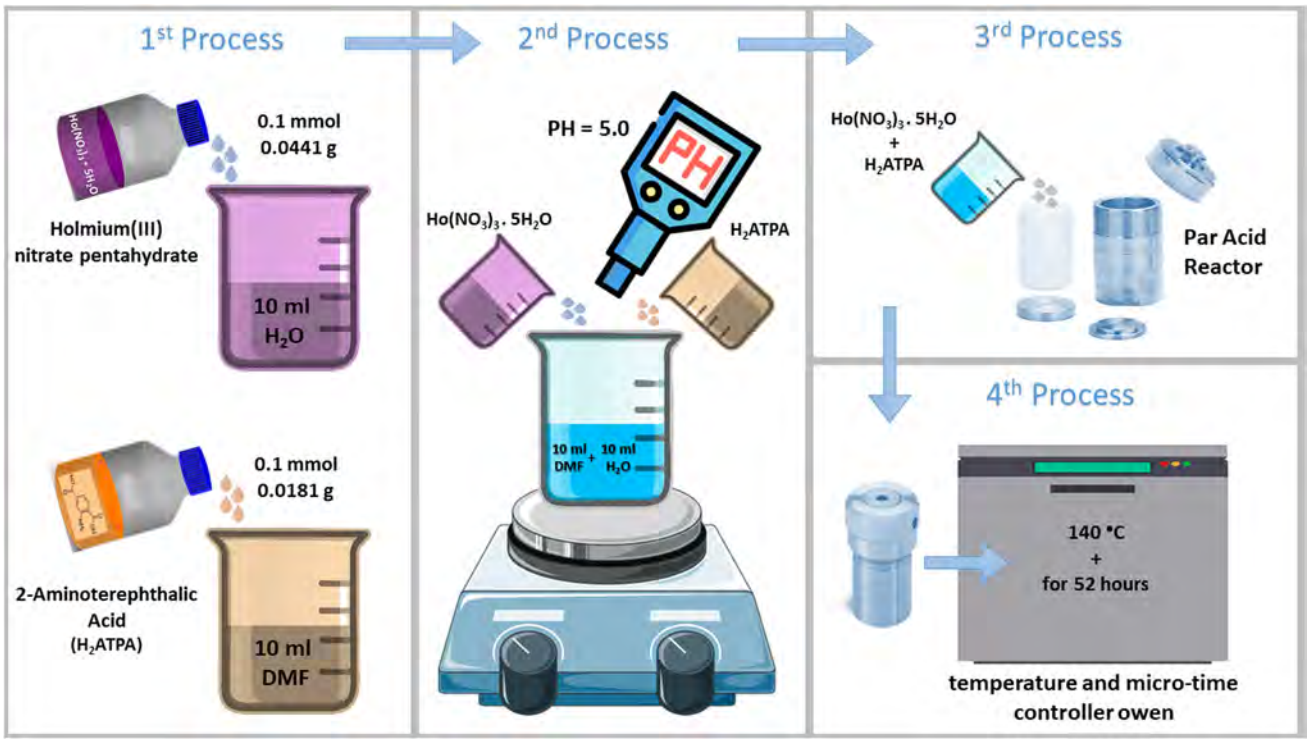

Scheme 2 Schematic illustration of synthesis route of **1**

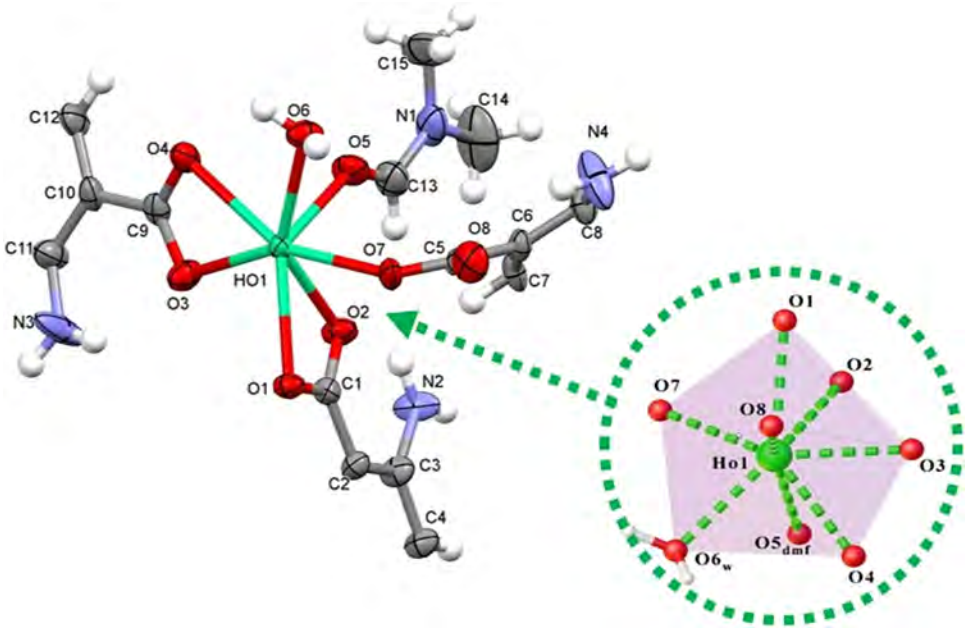

Fig. 1 Asymmetric unit of **1** showing thermal ellipsoids on the 50% probability level and corresponding atom labeling scheme and depicting the local coordination environment around the Ho(III) centre that adopts a distorted bicapped trigonal prismatic geometry. Atomic color scheme: Ho, green; O, red; N, blue; C, grey; H, white

behaving in μ_4-mode bridges two nearest Ho(III) centers, forming a dimeric Holmium unit as shown in Fig. 3. These Ho(III) dimers are linked through μ_4-bridging H_2ATPA linkers to give a 1D substructure (Fig. 4). Furthermore, adjacent chains are further associated together via the linear H_2ATPA exhibiting μ-chelation, resulting in a 3D extended framework in the *bc* plane associate into columnar stacks oriented along the *a* axis (Fig. 4). H_2-ATPA ligand is bound as a polydentate ligand to the Ho atoms and a 3D polymeric compound is formed which makes **1** is stable. The data in Table 3 were obtained from PLATON software [28]. The crystal structure of **1** is more stabilized by intermolecular N–H···O, N–H···N and O–H···O interactions (Table 3).

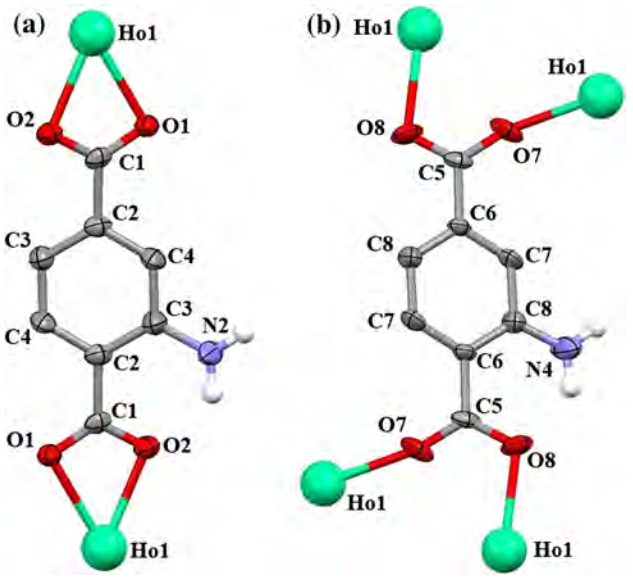

Fig. 2 Coordination modes of the 2-aminoterephtalic ligand (**a**) μ-$(\eta_2{:}\eta_2)$ and (**b**) μ_4-$(\eta_1{:}\eta_1{:}\eta_1{:}\eta_1)$ in **1**. Atomic color scheme: Ho, green; O, red; N, blue; C, grey; H, white

Table 2 The selected bond lengths (Å) and bond angles (°) for **1**

Ho1—O1	2.451 (3)	Ho1—O5	2.325 (3)
Ho1—O2	2.397 (3)	Ho1—O6	2.378 (3)
Ho1—O3	2.363 (3)	Ho1—O7	2.323 (3)
Ho1—O4	2.467 (3)	Ho1—$O8^{i}$	2.354 (3)
O1—Ho1—O4	134.92 (11)	O6—Ho1—O2	141.40 (12)
O2—Ho1—O1	53.82 (9)	O6—Ho1—O4	77.44 (11)
O2—Ho1—O4	117.11 (11)	O7—Ho1—O1	72.64 (11)
O3—Ho1—O1	83.58 (11)	O7—Ho1—O2	81.07 (12)
O3—Ho1—O2	75.05 (12)	O7—Ho1—O3	153.30 (12)
O3—Ho1—O4	53.76 (11)	O7—Ho1—O4	152.06 (12)
O3—Ho1—O6	131.02 (11)	O7—Ho1—O5	89.56 (12)
O5—Ho1—O1	126.60 (11)	O7—Ho1—O6	75.59 (12)
O5—Ho1—O2	74.20 (11)	$O8^{i}$—Ho1—O1	77.26 (11)
O5—Ho1—O3	95.19 (13)	$O8^{i}$—Ho1—O2	123.82 (12)
O5—Ho1—O4	76.61 (12)	$O8^{i}$—Ho1—O3	73.60 (12)
O5—Ho1—O6	75.30 (12)	$O8^{i}$—Ho1—O4	77.17 (12)
O5—Ho1—$O8^{i}$	153.16 (13)	$O8^{i}$—Ho1—O6	93.50 (12)
O6—Ho1—O1	140.52 (10)		

Symmetry code: (i) $-x+1, -y, -z+1$

FT-IR Spectra

To better understanding of the vibration process of the structure which we analyzed, the room temperature FT-IR spectra of **1** and its free ligand H_2ATPA, which is in very well agreement with the single-crystal structure analysis, have been measured in the range 4000–600 cm^{-1} and the obtained spectra have been compared with each other for suggesting possible vibrations mode as can be seen in Fig. 5. Except for a few vibration peaks, the other peaks present in both spectra are in almost similar regions. The first thing in the spectra discussed is that the presence of a weak sharp IR band around 3457 cm^{-1} confirms the existence of symmetric and asymmetric stretches of free NH_2 groups [23]. A weak broad vibration peak which corresponds to the ν(O–H) stretching vibrations of the coordinated water molecules observed that centered at around 3400 cm^{-1} for both spectra [29–32]. The weak vibration peak observed in ligand at 2625 cm^{-1}, which is not seen in the complex, is proved to be the presence of DMF molecules and the reason for this peak can be attributed to the aliphatic stretching vibrations of the C–H groups [33–36]. The characteristic intensive band of carbonyl υ(C=O) group is shifted from 1671 cm^{-1} for H_2-ATPA ligand to 1654 cm^{-1} for **1** [33]. There are two functional groups which are amine and carboxylate due to the presence of H_2ATPA ligand which is evident from IR spectra. The intensive IR bands in the range of 1529–1328 cm^{-1} can be assigned to antisymmetric and symmetric stretching vibrations of carboxylate groups are coordinated with the Ho(III) ions in the chelate mode while the stretching vibrations of amine group, which plays an important role in providing stability and robustness to the complex structures in hydrogen bonding, may be responsible for the weak bands at 3457 cm^{-1} and 3379 cm^{-1} [22, 33, 37]. In addition to all this, some characteristic vibration peaks are present in both spectra in the region of 1258–1110 cm^{-1} which may be attributed to the sulfonate groups are ν(S–O) and ν(C–S) vibrations [38, 39]. All of these observed peaks shift towards the lower wavenumber values with very little difference in the IR spectrum of the H_2ATPA ligand. For the interpreting of the lowest region of the peaks observed in the band of 848–670 cm^{-1} of the IR spectra, one can conclude that the peaks are caused by O–Ho–O and Ho–O stretching vibrations [12].

Solid State UV–Vis Spectra

The UV–Vis absorption spectra of free ligand H_2ATPA and Ho(III) compound, **1**, have been investigated in solid state and shown in Fig. 6. There has been one absorption band at 373 nm for the ligand while there has been one maximum at 493 nm for **1**. These near UV absorptions may be attributed π–π* or n–π* transition of the free ligand [39–45]. The bands have been slightly shifted towards lower energy which signifies the lanthanide ion coordination with H_2ATPA ligand [46].

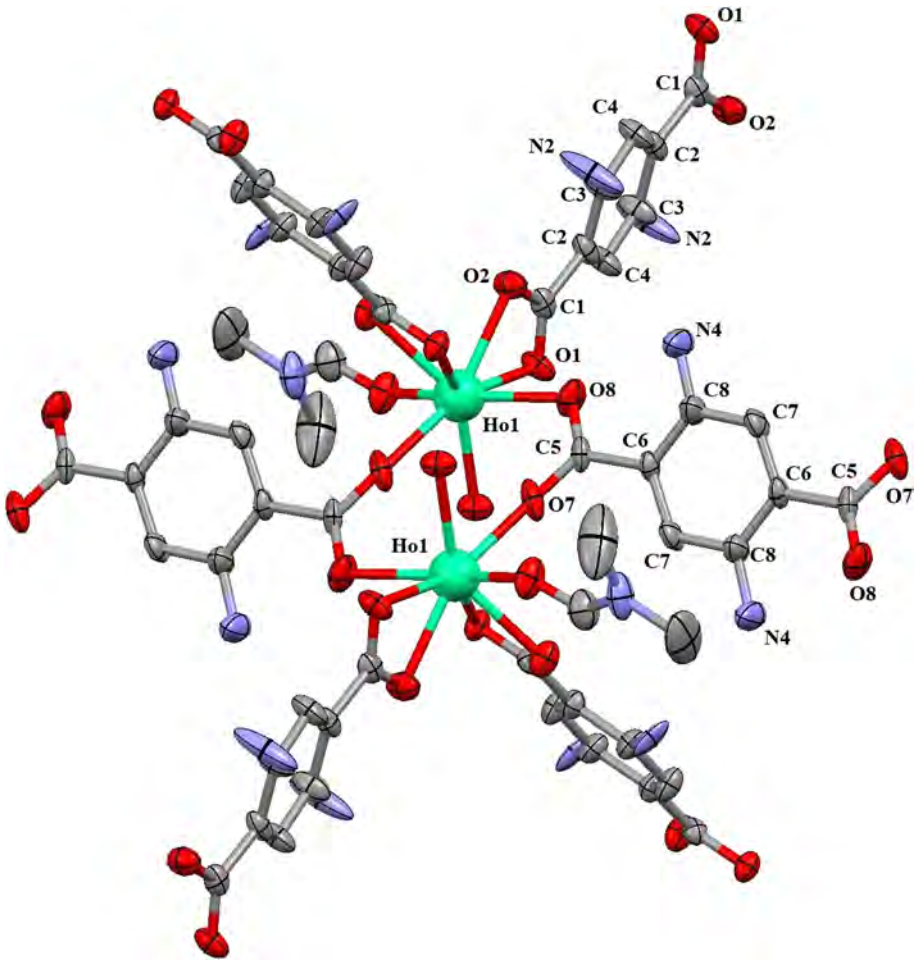

Fig. 3 Dimeric Ho(III) structural unit of **1**. H atoms were omitted for clarity. Atomic color scheme: Ho, green; O, red; N, blue; C, grey; H, white

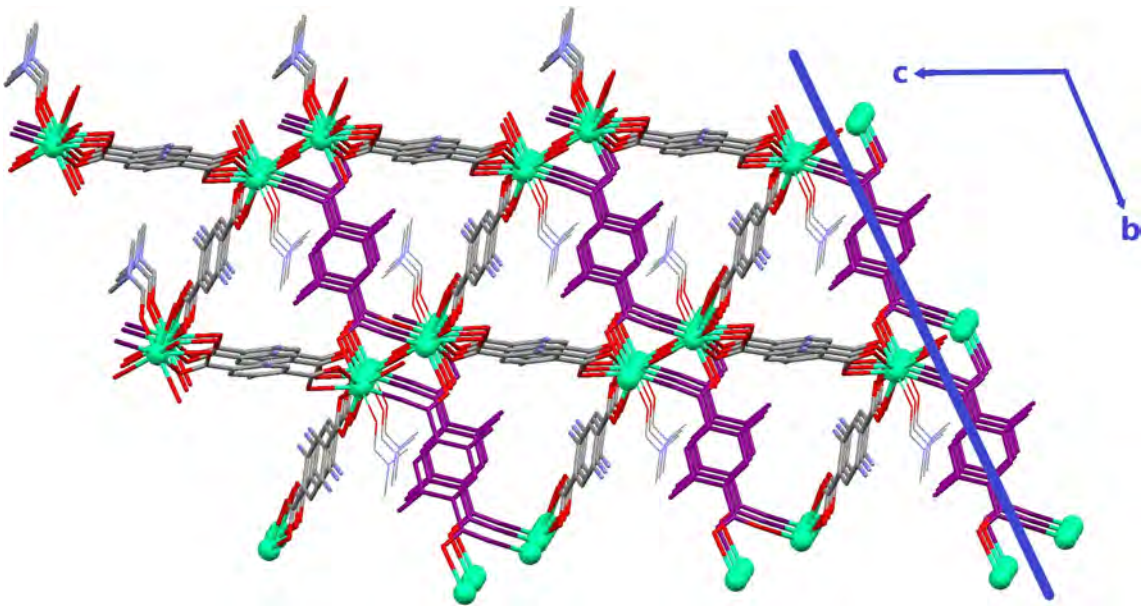

Fig. 4 Dimeric Holmium structural unit that forms the 3D extended framework of **1** in the *bc* plane associate into columnar stacks oriented along the *a*-axis. Ho(III) dimers are linked through μ_4-bridging H_2ATPA linkers (purple units) to give a 1D substructure (blue rod). H atoms were omitted for clarity. Atomic color scheme: Ho, green; O, red; N, blue; C, grey; H, white

Table 3 Hydrogen-bond geometry (Å, °) for **1**

D-H···A*	D-H	H···A	D···A	D-H···A	Symmetry
N2-H2A···O3	0.86	2.17	3.00	164	−x, 1−y, −z
N2-H2B···O2	0.86	1.87	2.54	133	1−x, 1−y, 1−z
N3-H3A···O8	0.86	2.44	3.27	162	−1−x, 2−y, 1−z
N3-H3B···O3	0.86	2.03	2.63	127	2−x, 2−y, −z
N3-H3B···N3	0.86	2.36	3.02	134	1−x, 1−y, −z
N4-H4A···N2	0.86	2.54	3.36	162	−1−x, 2−y, −z
N4-H4B···N3	0.86	1.99	2.56	123	2−x, 2−y, 1−z
N4-H4B···O8	0.86	2.07	2.69	128	−1 + x, y, z
O6-H6B···O1	0.86	1.93	2.77	169	x, y, −1 + z
O6-H6B···O7	0.86	2.53	2.98	114	x, y, 1 + z

*D donor, A acceptor

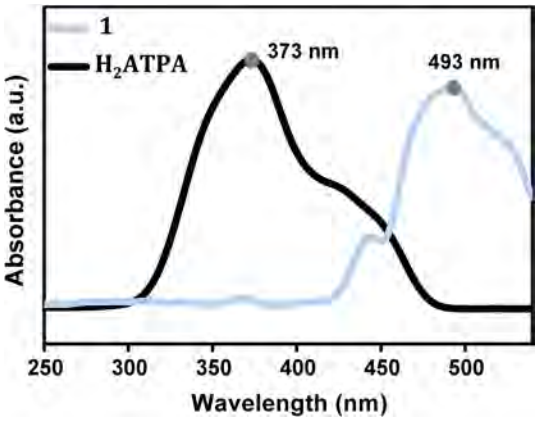

Fig. 6 The solid-state UV–Vis spectra of the free ligand H_2ATPA (black solid line) and **1** (blue solid line)

Photoluminescence Spectra

Recently emissive coordination polymers are of great interest due to their various applications in the photochemistry area as a chemical and biological sensor. The solid-state photoluminescence (PL) measurements have been taken at room temperature under the excitation at 349 nm for discovering the whole emission and energy-transfer process of **1** and its free ligand H_2ATPA. A broad bright-yellow emission peak at $\lambda_{max} = 585$ nm has appeared in the PL spectrum of the free H_2ATPA ligand as shown in Fig. 7a. This behavior may be related to the $n \rightarrow \pi^*$ or $\pi \rightarrow \pi^*$ inter-ligand electronic transition (ILCT) [47, 48]. In comparison, four Ho-based characteristic emission bands due to the f–f transitions of Ho(III) ion have been seen after complexation in the region 400–750 nm as shown in Fig. 7b. The narrow strong emission bands at 442 nm and 464 nm which can be interpreted as $^5G_5 \rightarrow {}^5I_8$ and $^5G_6 \rightarrow {}^5I_8$ transitions much more intensive than the emission bands at 643 nm and 660 nm which can correspond to $^5G_4 \rightarrow {}^5I_6$ and $^5F_5 \rightarrow {}^5I_8$ transitions for the visible region, respectively [14, 33, 49]. Therefore, the investigated complex emits the bright-blue light.

While the curves of the emission bands of the organic chromophores are usually broad and splayed, the curves of the emission bands obtained from lanthanide-based materials are narrow and strong due to the f–f transitions caused by the emitting state of the Ln(III) ion. Because the free ligands act as strong sensitizer and the excitation energy transfers effectively from the ligands to the lanthanide ions, the emission bands observed in the free organic H_2ATPA ligand cannot be expected to appear in the emission spectrum of **1** obtained after synthesized with Ho(III) ions. In the literature, it can be easily concluded that the coordinated water may eliminate the emission of Ho(III) ion, but

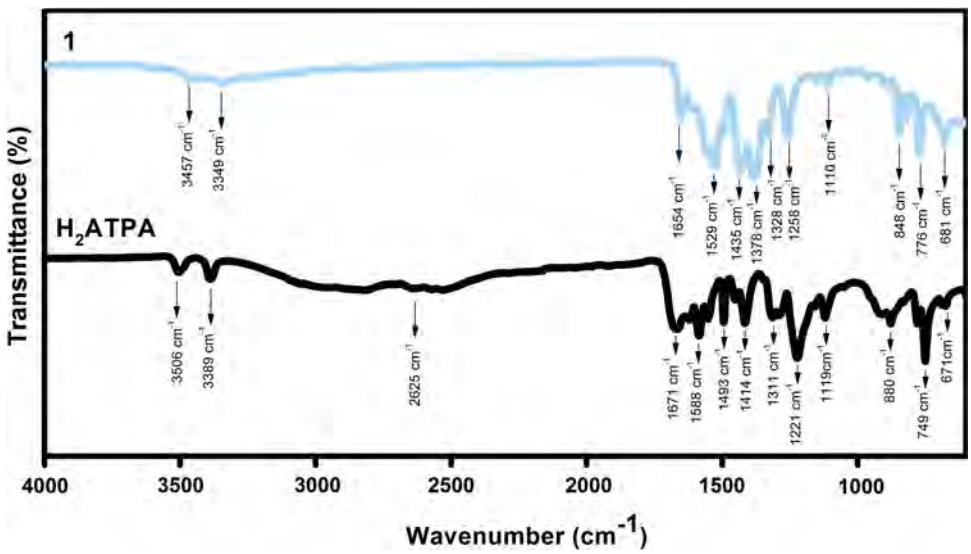

Fig. 5 The FT-IR spectra of the free ligand H_2ATPA (black solid line) and **1** (blue solid line)

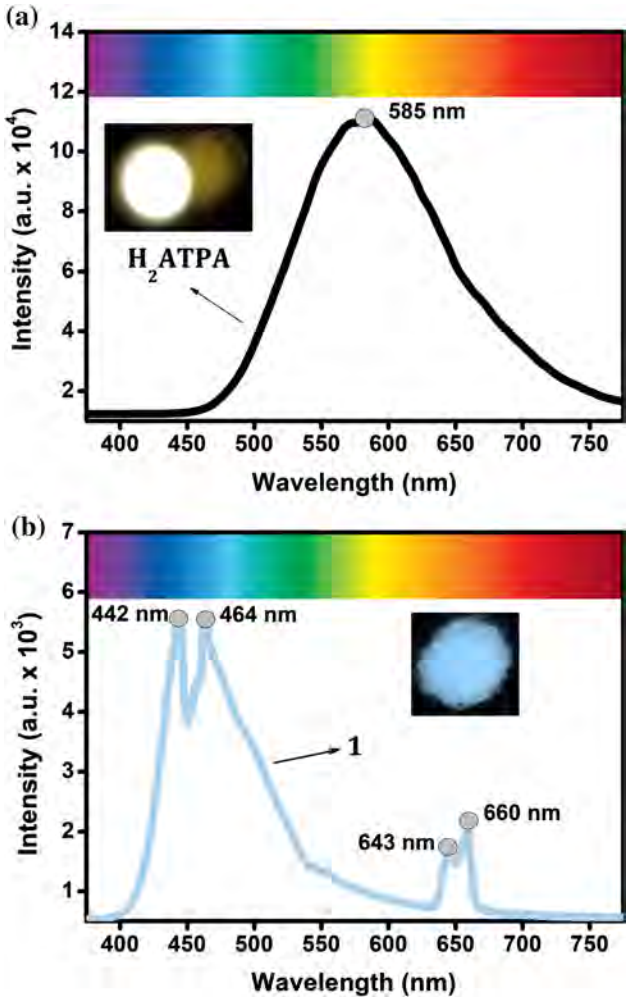

Fig. 7 Room-temperature solid-state photoluminescence spectrum of **(a)** H_2ATPA (black solid line). The upper-left photo is the photoluminescent image of the free ligand while excited at 349 nm, and **(b) 1** (blue solid line). The upper-right photo is the photoluminescent image of **1** while excited at 349 nm

in our case **1** presents intense bright-blue emission. This effect may be explained by the sensitization of the ligand. The ligand-to-metal charge transfer (LMCT) may be responsible for these transitions which are consistent with the emission spectra reported in previous studies on Ho(III)-based compounds [11–14, 50].

In the last quarter of a century when technology has developed rapidly, one of the most effective strategies for the growth or generate the highly luminescent sensors is the addition of the lanthanide ions into a multifunctional supramolecular scaffold. Since ions such as Ho(III) are present in spectrally narrow emission, they are a priority candidate in such matters. The electronic transitions that cause photon emission by the 5d shell are limited. Therefore, very little expansion may occur caused by solvation. On the other hand, since lanthanides are naturally characterized as hard acids, diffuse interactions leading to line expansion can be attributed negatively. Unfortunately, the direct excitation of lanthanide ions is nearly impossible. The reason for this phenomenon is that the f–f transitions are prohibited due to parity (Laporte) selection rules. This result leads to weak absorbance and low quantum yields. One of the most transitional ways to overcome from this issue can be accomplished by the complex formation of the desired lanthanide involved with a strongly absorbent linker. In this case, in the light of strong vibrating coupling between the metal ions and the liker, direct energy transfer from the excited state of the more readily accessible linker to the appropriate metal energy level can be achieved. The coupling obtained at the end of all this process causes an increase in luminescence, which is known as the antenna effect [13, 51, 52].

The energy level diagram and energy transfer mechanism for **1** is shown in Fig. 8. The lanthanide-sensitization process takes place in three different steps. The first step, when **1** induced by certain radiation, H_2ATPA ligand absorbs all the energy then is excited from the ground state to the higher energy level which is called singlet (S1) excited state. After this, in the second step, the energy of the excited state S1 is transferred to its triplet (T1) energy state. This happens through the inter-system crossing (ISC) process which causes usual path for energy transfer from H_2ATPA ligand to Ho(III) ions. The final step is the transfer of energy to the 4f levels of the Ho(III) ions. In this step, an energy level which is the energy difference between the excited energy level of the H_2ATPA ligand and the triplet state of the Ho(III) ions play a key role in efficient energy transfer [53–55]. If the energy difference between these two states is too high, the overlapping of the triplet energy state of the ligand and Ho(III) ions will decrease and the energy transfer will drop sharply. If the difference between the triplet energy state is too small, then the transfer process of the ligand from Ho(III)-based lanthanide ions will starts. In our study, it can be easily concluded that the energy transfers from the H_2ATPA ligand to Ho(III) have been done effectively so that **1** would have the potential applications in the optical amplification field.

Conclusion

A new Ho(III)—cluster-based 3D coordination polymer **1**, $\{Ho_2(H_2O)_2(DMF)_2(ATPA)_3\}_n$, has been successfully synthesized using the hydrothermal method. The structural and photoluminescence properties of **1** have been characterized by elemental analysis, FT-IR, UV, single crystal and powder X-ray diffraction and photoluminescence measurement techniques. Single crystal X-ray diffraction results indicated that each Ho(III) atom adopts a distorted bicapped trigonal prismatic geometry which formed by

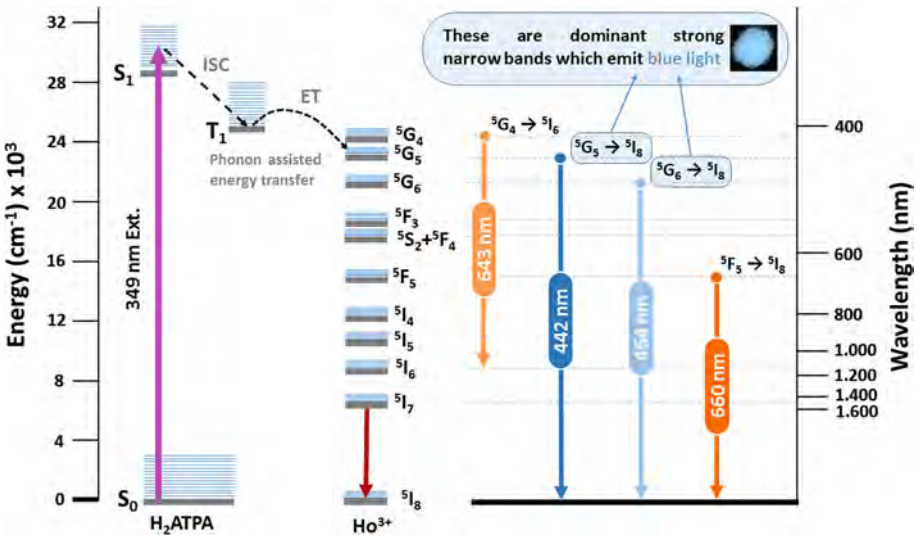

Fig. 8 The schematic diagram for the sensitization mechanism of the Ho(III) ion by H_2ATPA ligand (left) and energy level diagrams of Ho(III) ion

eight oxygen atoms. The coordination of Ho(III) ions with H_2ATPA ligand has been confirmed by the red shifting of the absorption band in the UV–Visible spectra. Four Ho(III)-based characteristic narrow strong emission bands attributed to the f–f transitions of Ho(III) cation were detected for **1** in the visible region. The emission spectrum of **1** reveals intense bright-blue emission in the visible region. It may easily be concluded from the solid-state photoluminescence measurements that utilizing sensitization processing due to strong intramolecular energy transfer from H_2ATPA ligand which can show that **1** would have great potential applications in the optical amplification field. This research which contains luminescence study indicates 2-aminoterephthalate ligand may pave the way for the Ho-based lanthanide-organic frameworks as the luminescent probes applied in detection and photonic applications, and it is believed that the strategy employed herein can further propel the development of multifunctional MOFs sought for applicability as optical sensors.

Supplementary Material

CCDC- 1855892 contains the supplementary crystallographic data for the **1**. This data can be obtained free of charge from The Cambridge Crystallographic Data Center Via http://www.ccdc.cam.ac.uk/data_request/cif.

Acknowledgment This paper has been granted by the Muğla Sıtkı Koçman University Research Projects Coordination Office through Project Grant Number: (17/295). The author is grateful to the Dokuz Eylul University for the use of the Agilent Xcalibur Eos diffractometer and acknowledges Balıkesir University, Science and Technology Application and Research Center (BUBTAM), for the use photoluminescence measurements. The author is very thankful to Dr. Hülya Kara SUBAŞAT, Dr. Uğur ERKARSLAN, Dr. M. Burak ÇOBAN and Dr. Çiğdem Elif DEMİRCİ DÖNMEZ for their helpful and constructive suggestions.

References

1. N. L. Torad, Y. Li, S. Ishihara, K. Ariga, Y. Kamachi, H. Y. Lian, H. Hamoudi, Y. Sakka, W. Chaikittisilp, K. C. W. Wu, and Y. Yamauchi (2014). *Chem. Lett.* **43**, 717.
2. W. Zhang, X. Jiang, X. Wang, Y. V. Kaneti, Y. Chen, J. Liu, J. Sen Jiang, Y. Yamauchi, and M. Hu (2017). *Angew Chemie Int. Ed.* **56**, 8435.
3. C. Young, R. R. Salunkhe, J. Tang, C. C. Hu, M. Shahabuddin, E. Yanmaz, M. S. A. Hossain, J. H. Kim, and Y. Yamauchi (2016). *Phys. Chem. Chem. Phys.* **18**, 29308.
4. A. Azhar, Y. Li, Z. Cai, M. B. Zakaria, M. K. Masud, M. S. A. Hossain, J. Kim, W. Zhang, J. Na, Y. Yamauchi, and M. Hu (2019). *Bull. Chem. Soc. Jpn.* **92**, 875.
5. G. E. Gomez, E. V. Brusau, J. Sacanell, G. J. A. A. Soler Illia, and G. E. Narda (2018). *Eur. J. Inorg. Chem.* **2018**, 2452.
6. S. Wu, Y. Lin, J. Liu, W. Shi, G. Yang, and P. Cheng (2018). *Adv. Funct. Mater.* **28**, 1.
7. J. X. Ma, J. Guo, H. Wang, B. Li, T. Yang, and B. Chen (2017). *Inorg. Chem.* **56**, 7145.
8. W. Xu, Y. Lou, W. Chen, and Y. Kang (2019). *Biomed. Eng./ Biomed. Tech.* **1**, 1.
9. M. A. Chowdhury (2017). *ChemBioEng Rev.* **4**, 225.
10. U. Erkarslan, A. Donmez, H. Kara, M. Aygun, and M. B. Coban (2018). *J. Clust. Sci.* **29**, 1177.
11. M. B. Coban, U. Erkarslan, G. Oylumluoglu, M. Aygun, and H. Kara (2016). *Inorganica Chim. Acta* **447**, 87.
12. A. Dönmez (2018). *Mugla J. Sci. Technol.* **4**, 116.
13. M. B. Coban, A. Amjad, M. Aygun, and H. Kara (2017). *Inorganica Chim. Acta* **455**, 25.
14. G. Oylumluoglu, M. B. Coban, C. Kocak, M. Aygun, and H. Kara (2017). *J. Mol. Struct.* **1146**, 356.
15. Y. Cui, J. Zhang, B. Chen, and G. Qian (2016). *Handb. Phys. Chem. Rare Earths* **50**, 243.
16. J. Rocha, L. D. Carlos, F. A. A. Paz, and D. Ananias (2011). *Chem. Soc. Rev.* **40**, 926.
17. Z. Dou, J. Yu, Y. Cui, Y. Yang, Z. Wang, D. Yang, and G. Qian (2014). *J. Am. Chem. Soc.* **136**, 5527.

18. S. E. Miller, M. H. Teplensky, P. Z. Moghadam, and D. Fairen-Jimenez (2016). *Interface Focus* **6**, 1.
19. S. Ma, D. Yuan, X. Sen Wang, and H. C. Zhou (2009). *Inorg. Chem.* **48**, 2072.
20. H. N. Abdelhamid, M. Wilk-Kozubek, A. M. El-Zohry, A. Bermejo Gómez, A. Valiente, B. Martín-Matute, A. V. Mudring, and X. Zou (2019). *Microporous Mesoporous Mater.* **279**, 400.
21. P. Y. Du, W. Gu, and X. Liu (2016). *New J. Chem.* **40**, 9017.
22. M. Kariem, M. Yawer, S. Sharma, and H. N. Sheikh (2016). *ChemistrySelect* **1**, 4489.
23. J. H. Liao, C. S. Tsai, and T. K. Lin (2010). *Inorg. Chem. Commun.* **13**, 286.
24. G. M. Sheldrick (2008). *Acta Crystallogr. Sect. A Found. Crystallogr.* **64**, 112.
25. G. M. Sheldrick (2015). *Acta Crystallogr. Sect. C Struct. Chem.* **71**, 3–8.
26. O. V. Dolomanov, L. J. Bourhis, R. J. Gildea, J. A. K. Howard, and H. Puschmann (2009). *J. Appl. Crystallogr.* **42**, 339.
27. A. Dikhtiarenko, P. Serra-Crespo, S. Castellanos, A. Pustovarenko, R. Mendoza-Merono, S. García-Granda, and J. Gascon (2016). *Cryst. Growth Des.* **16**, 5636.
28. A. L. Spek (2009). *Acta Crystallogr. D. Biol. Crystallogr.* **65**, 148.
29. E. Gungor and H. Kara (2011). *Spectrochim Acta Part A Mol. Biomol. Spectrosc.* **82**, 217.
30. E. Gungor, H. Kara, E. Colacio, and A. J. Mota (2014). *Eur. J. Inorg. Chem.* **2014**, 1552.
31. E. Gungor, Y. Yahsi, H. Kara, and A. Caneschi (2015). *Cryst. Eng. Commun.* **17**, 3082.
32. H. Kara, A. Karaoglu, Y. Yahsi, E. Gungor, A. Caneschi, and L. Sorace (2012). *Cryst. Eng. Commun.* **14**, 7320.
33. M. Almáši, V. Zeleňák, L. Galdun, and J. Kuchár (2014). *Inorg. Chem. Commun.* **39**, 39.
34. D. A. Kara, A. Donmez, H. Kara, and M. Burak Coban (2018). *Acta Crystallogr. Sect. C Struct. Chem.* **74**, 901.
35. C. Kocak, G. Oylumluoglu, A. Donmez, M. B. Coban, U. Erkarslan, M. Aygun, and H. Kara (2017). *Acta Crystallogr. Sect. C Struct. Chem.* **73**, 414.
36. P. Chakraborty, I. Majumder, K. S. Banu, B. Ghosh, H. Kara, E. Zangrando, and D. Das (2016). *Dalt. Trans.* **45**, 742.
37. C. F. De Almeida, R. C. De Andrade, L. W. Aguiar, F. J. Caires, E. A. Falcão, and C. T. De Carvalho (2014). *J. Therm. Anal. Calorim.* **117**, 251.
38. X. Li, Z. Xie, J. Lin, and R. Cao (2009). *J. Solid State Chem.* **182**, 2290.
39. X. Li, Y. Lu, Y. Bing, and M. Q. Zha (2012). *Synth. React. Inorganic Met. Nano-Metal Chem.* **42**, 698.
40. A. Donmez, G. Oylumluoglu, M. B. Coban, C. Kocak, M. Aygun, and H. Kara (2017). *J. Mol. Struct.* **1149**, 569.
41. A. Donmez, M. B. Coban, C. Kocak, G. Oylumluoglu, U. Baisch, and H. Kara (2017). *Mol. Cryst. Liq. Cryst.* **652**, 213.
42. A. Donmez, M. B. Coban, and H. Kara (2018). *J. Clust. Sci.* **29**, 951.
43. E. Otgonbaatar, M.-C. Chung, K. Umakoshi, and C.-H. Kwak (2015). *J. Nanosci. Nanotechnol.* **15**, 1389.
44. S. Yoopensuk, P. Tongying, K. Hansongnern, C. Pakawatchai, S. Saithong, Y. Tantirungrotechai, and N. Leesakul (2012). *Spectrochim. Acta Part A Mol. Biomol. Spectrosc.* **86**, 538.
45. U. Erkarslan, G. Oylumluoglu, M. B. Coban, E. Öztürk, and H. Kara (2016). *Inorganica Chim. Acta* **445**, 57.
46. S. Alghool, M. S. Zoromba, and H. F. A. El-Halim (2013). *J. Rare Earths* **31**, 715.
47. Y. Yahsi, H. Ozbek, M. Aygun, and H. Kara (2016). *Acta Crystallogr. Sect. C Struct. Chem.* **72**, 426.
48. S. Chooset, A. Kantacha, K. Chainok, and S. Wongnawa (2018). *Inorganica Chim. Acta* **471**, 493.
49. B. C. F. Farinelli, M. S. Silva, E. R. Botero, C. T. Carvalho, A. R. L. Caires, R. Guo, A. S. Bhalla, and E. A. Falcão (2016). *Integr. Ferroelectr.* **174**, 167.
50. S. Dang, J. Yu, X. Wang, L. Sun, R. Deng, J. Feng, W. Fan, and H. Zhang (2011). *J. Lumin.* **131**, 1857.
51. M. D. Allendorf, C. A. Bauer, R. K. Bhakta, and R. J. T. Houk (2009). *Chem. Soc. Rev.* **38**, 1330.
52. Y. Cui, B. Chen, and G. Qian (2014). *Coord. Chem. Rev.* **273–274**, 76.
53. S. Dang, L. N. Sun, H. J. Zhang, X. M. Guo, Z. F. Li, J. Feng, H. D. Guo, and Z. Y. Guo (2008). *J. Phys. Chem. C* **112**, 13240.
54. N. Sabbatini, A. Mecati, M. Guardigli, V. Balzani, J. M. Lehn, R. Zeissel, and R. Ungaro (1991). *J. Lumin.* **48–49**, 463.
55. D. L. Dexter (1953). *J. Chem. Phys.* **21**, 836.